Invited Article
Chinese Science Bulletin
Condensed Matter Physics
October 2012 Vol. 57 No. 30: 3829–3835
doi: 10.1007/s11434-012-5405-7

The orbital characters of low-energy electronic structure in iron-chalcogenide superconductor $K_xFe_{2-y}Se_2$

CHEN Fei[1], GE QingQin[1], XU Min[1], ZHANG Yan[1], SHEN XiaoPing[1], LI Wei[2], MATSUNAMI Masaharu[3], KIMURA Shin-ichi[3], HU JiangPing[4,5] & FENG DongLai[1*]

[1] *State Key Laboratory of Surface Physics, Department of Physics, and Advanced Materials Laboratory, Fudan University, Shanghai 200433, China;*
[2] *Department of Physics, Fudan University, Shanghai 200433, China;*
[3] *UVSOR Facility, Institute for Molecular Science and The Graduate University for Advanced Studies, Okazaki 444-8585, Japan;*
[4] *Department of Physics, Purdue University, West Lafayette, Indiana 47907, USA;*
[5] *Beijing National Laboratory for Condensed Matter Physics, Institute of Physics, Chinese Academy of Sciences, Beijing 100080, China*

Received April 20, 2012; accepted June 26, 2012; published online August 10, 2012

The newly discovered iron-chalcogenide superconductor $K_xFe_{2-y}Se_2$ exhibits a distinct electronic structure from other iron-based superconductors. Exploiting polarization-dependent angle-resolved photoemission spectroscopy, we have determined the orbital characters of band structure in a $K_xFe_{2-y}Se_2$ superconductor. To a large extent, we find that $K_xFe_{2-y}Se_2$ superconductor shares similar orbital characters with other iron-based superconductors, but with its own characteristics. For example, we have resolved two highly degenerate electron cylinders around the zone corner in the *s* and *p* geometries, respectively, indicating negligible interactions between them. Moreover, in contrast to the band calculation results, the small electron pocket around *Z* is found to be mainly consisted of the d_{z^2} orbital. The determined orbital characters would help to construct a realistic model for $K_xFe_{2-y}Se_2$.

iron-chalcogenide superconductor, electronic structure, angle-resolved photoemission spectroscopy

Citation: Chen F, Ge Q Q, Xu M, et al. The orbital characters of low-energy electronic structure in iron-chalcogenide superconductor $K_xFe_{2-y}Se_2$. Chin Sci Bull, 2012, 57: 3829–3835, doi: 10.1007/s11434-012-5405-7

$K_xFe_{2-y}Se_2$, an iron-chalcogenide superconductor, exhibits many unique properties that distinguish itself from other iron-based superconductors [1]. While the parent compounds of most iron-based superconductors are metallic [2–4], the parent compound of $K_xFe_{2-y}Se_2$ superconductor is found to be either insulating or semiconducting [5–9]. The insulating parental phase even exhibits certain Mott-insulator signatures, and it is phase separated from the superconducting phase in the $K_xFe_{2-y}Se_2$ superconductor at a mesoscopic scale [7, 10]. Moreover, angle-resolved photoemission spectroscopy (ARPES) studies have shown that its Fermi surface is consisted of electron pockets only [7, 11, 12], which is again distinct from most of the iron-based superconductors [13–17]. These unique properties of $K_xFe_{2-y}Se_2$ have raised a lot of interest. Since the low-energy electronic structures of the iron-based superconductors are dominated by multiple 3*d* orbitals [18–20], the orbital degree of freedom is known to play an important role in the superconductivity of iron-based superconductors. For example, our recent ARPES study on $BaFe_2(As_{1-x}P_x)_2$ indicates that the nodal superconducting gap there is likely induced by the strong mixing of the d_{z^2} orbital into a hole-like band [21]. Therefore, to comprehend the unique properties of $K_xFe_{2-y}Se_2$, one needs to determine its low-energy electronic structure, particularly the orbital characters.

The sensitive response of different 3*d* orbitals in a polarization-dependent ARPES measurement makes it a powerful tool to explore the multi-orbital band structure of iron-based superconductors [22]. Polarization-dependent ARPES experiments have been conducted extensively on the iron-based superconductors, including LaOFeAs [13], $BaFe_2As_2$ [23–27], NaFeAs [28, 29], and FeTe [17, 27]. Here

*Corresponding author (email: dlfeng@fudan.edu.cn)

we report the polarization-dependent ARPES study on the orbital characters of $K_xFe_{2-y}Se_2$ superconductor. The orbital characters of low-energy electronic structure have been determined. Specifically, we found that the small electron pocket near the Z point is mostly dominated by the d_{z^2} orbital, and the large Fermi cylinders around the zone corner are actually contributed by two bands with highly degenerate Fermi crossings. One of the two bands is dominated by the d_{xz} and d_{yz} orbitals, while the other one is dominated by the d_{xy} orbital. The weak interactions between these two Fermi cylinders suggest that even if the superconducting order parameters on them have opposite signs, gap nodes would be absent [30,31]. Our results provide a foundation for the understanding and realistic modeling of $K_xFe_{2-y}Se_2$.

1 Experimental

$K_xFe_{2-y}Se_2$ single crystals were synthesized by self-flux method as described elsewhere in detail [32]. The samples show flat shiny surfaces with black color, and their element compositions were determined through energy-dispersive X-ray (EDX) analysis as $K_{0.75}Fe_{1.69}Se_2$. All the polarization-dependent photoemission data have been taken with an MBS A-1 analyzer at Beamline 7 of the ultraviolet synchrotron orbital radiation facility (UVSOR), and other photoemission data were taken with a Scienta electron analyzer at the Beamline 5-4 station of the Stanford Synchrotron Radiation Lightsource (SSRL). The overall energy resolution is set to be 15 meV or better, and the typical angular resolution is 0.3 degree. The samples were all cleaved *in situ* and measured at 35 K under ultra-high-vacuum better than 3×10^{-11} torr.

In a polarization-dependent ARPES measurement, the photoemission intensity is given by

$$|M^{\boldsymbol{k}}_{f,i}| \propto |\langle\phi^{\boldsymbol{k}}_f|\hat{\varepsilon}\cdot\boldsymbol{r}|\phi^{\boldsymbol{k}}_i\rangle|^2,$$

where $\hat{\varepsilon}$ is the unit vector of the electric field of the light, $\phi^{\boldsymbol{k}}_i$ is the initial-state wave funciton, and $\phi^{\boldsymbol{k}}_f$ is the final-state wave function which can be approximated by a plane-wave state $e^{i\boldsymbol{k}\cdot\boldsymbol{r}}$ with $\boldsymbol{k}$ in the mirror plane for the experimental setup in Figure 1(a). Here the analyzer slit and the sample surface normal define a mirror plane and the p (or s) experimental setup corresponds to the $\hat{\varepsilon}$ which is parallel (or perpendicular) to the mirror plane. Considering the spatial symmetries of the 3d orbitals (Figure 1(b)), when the analyzer slit is along the high-symmetry direction of the sample, the photoemission signal of certain orbitals would appear or disappear by specifying the polarization directions as summarized in Table 1. More detailed information about the polarization-dependent ARPES could be found in [23,28].

Since there are two types of locations for the selenium ions, one unit cell contains two iron ions. We define the x and y directions to be the two nearest-neighboring Fe-Fe bond directions in Figure 1(c), and the corresponding two-dimensional projected Brillouin zone (solid lines) and unfolded one for one iron ion per unit cell (dashed lines) are shown in Figure 1(d). Two high symmetry directions, $\Gamma(Z)$-$M(A)$ and $\Gamma(Z)$-$X(R)$, are labeled by #1 and #2, respectively, in Figure 1(d).

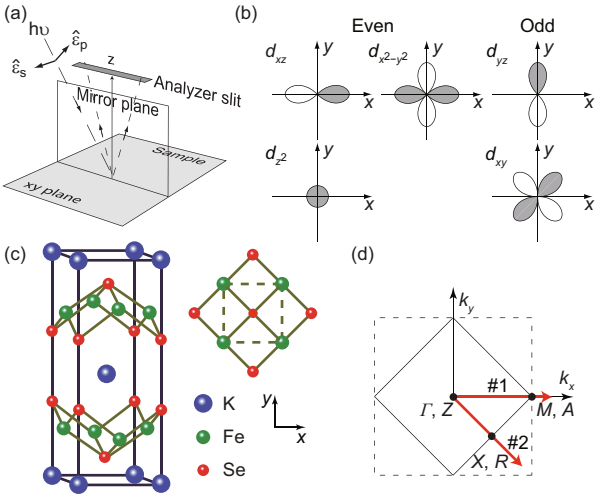

Figure 1 (Color online) (a) Experimental setup for polarization-dependent ARPES. (b) Illustration of the spatial symmetry of the 3d orbital with respect to the xz plane. (c) The schematic crystal structure of $K_xFe_{2-y}Se_2$ superconductor. The right side is the top view of the FeSe trilayer, and the x and y axes are along the two Fe-Fe bond directions. (d) Two-dimensional projection of the Brillouin zone (solid line) and the unfolded Brillouin zone (dashed line) [23].

Table 1 The possibility to detect the 3d orbitals along two high symmetry directions in the p and s geometries, respectively, by polarization-dependent APRES [23]

High-symmetry direction	Experimental geometry	3d orbitals				
		d_{xz}	$d_{x^2-y^2}$	d_{z^2}	d_{yz}	d_{xy}
#1 $\Gamma(Z)$-$M(A)$	p	√	√	√		
	s				√	√
#2 $\Gamma(Z)$-$X(R)$	p	√		√	√	√
	s	√	√		√	

2 Electronic structure around the zone center

The photoemission data taken around Γ are shown in Figure 2. In Figure 2(a), the upper panels are the photoemission spectra taken along Γ-M (#1) direction in the s and p geometries, respectively, and the lower panels are the corresponding second derivatives with respect to energy. Figure 2(b) is similar to Figure 2(a), except that the data were taken along Γ-X (#2) direction. We could resolve three hole-like bands, α, β, and γ, one electron-like band, ϵ, and two rather flat bands, ω and ω', around Γ in Figure 2.

The band assigned as α only emerges in the p geometry along both #1 and #2 directions, and could not be observed in the s geometry, which indicates its d_{xz} or d_{z^2} orbital character based on Table 1. The β band shows opposite spatial symmetry, as it could only be observed in the s geometry, thus

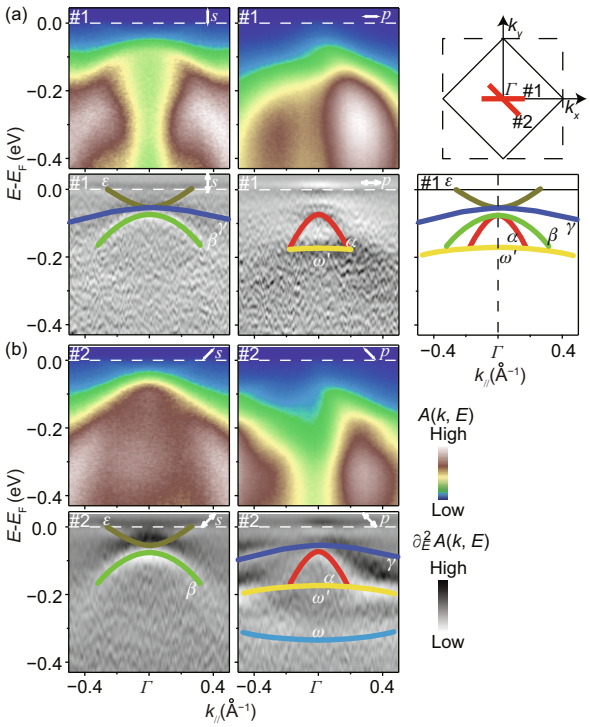

Figure 2 (Color online) The polarization-dependent APRES data around Γ taken with 21 eV photon. (a) The photoemission spectra and their corresponding second derivatives with respect to energy taken in the s and p geometries, respectively, along Γ-M direction. (b) is the same as the panel (a), but taken along Γ-X direction. The inset is the illustration of the cuts along Γ-M (#1) and Γ-X (#2) directions and the band structure along Γ-M direction.

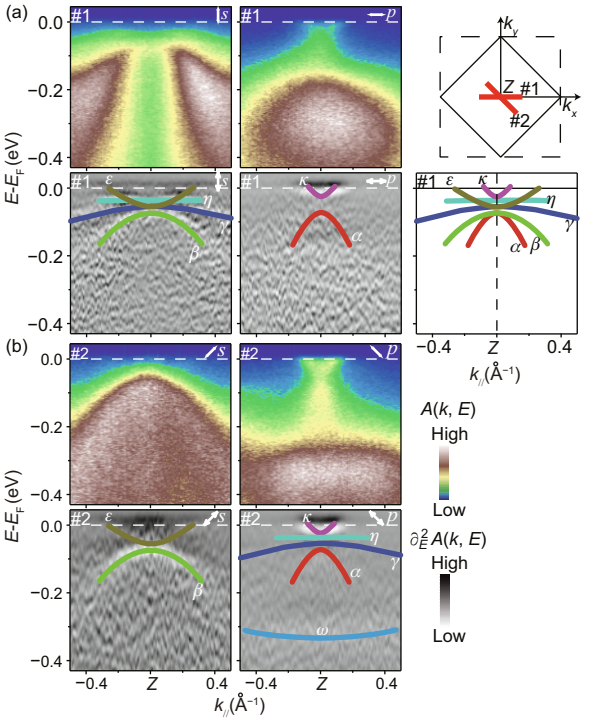

Figure 3 (Color online) The polarization-dependent APRES data around Z taken with 30 eV photon. (a) The photoemission spectra and their corresponding second derivatives with respect to energy taken in the s and p geometries, respectively, along Z-A direction. (b) is the same as the panel (a), but taken along Z-R direction. The inset is the illustration of the cuts along Z-A (#1) and Z-R (#2) directions and the band structure along Z-A direction.

we attribute it to d_{yz} according to Table 1. The band tops of α and β are below E_F and degenerate with each other at the Γ point. Note that, the tops of the bands with the d_{xz} and d_{yz} orbitals should have the same binding energy at the Γ point due to the four-fold symmetry of the lattice. Therefore, we attribute the α band to the d_{xz} orbital. The d_{xz} and d_{yz} orbitals have mixed symmetry along the Γ-X direction, and the strong polarization dependence here might be caused by the hybridization of d_{xz} and d_{yz} [23]. For the γ band, it emerges in the s geometry along #1 direction, and the p geometry along #2 direction, which is consistent with the symmetry of the d_{xy} orbital. In addition, an electron-like band, ϵ, only emerges in the s geometry along both directions with weak intensity, thus we attribute it to the d_{yz} orbital along the Γ-M direction. We will discuss its origin later.

Figure 3 shows the polarization-dependent data around the Z point. Four bands (α, β, γ, and ε) exhibit no energy shift or orbital character change compared with those around the Γ point. However, we have observed another two bands, κ and η, around the Z point. The κ band exhibits strong k_z dependence and its Fermi surface surrounds the Z point [7, 11]. It only emerges in the p geometry along both #1 and #2 directions, so it could be either d_{xz} or d_{z^2}. If the κ band is merely consisted of d_{z^2}, it would not show up in the s geometry. However, there indeed exist two pieces of weak Fermi arcs around Z in the s geometry (Figure 5(a)), thus the κ band should carry some d_{xz} character. Meanwhile, the overwhelmingly strong intensity in the p geometry over that in the s geometry suggests that the κ band should be dominated by the d_{z^2} orbital, with some trace of the d_{xz} orbital, and thus some d_{yz} as required by symmetry. On the other hand, the dispersiveless η band is neither predicted by theory or discovered in previous ARPES experiments. It behaves similarly as the γ band, so it might be consisted of the d_{xy} orbital as well.

In Figures 2 and 3, we could observe two rather flat bands assigned as ω' and ω at about 190 and 330 meV below E_F, respectively. Both bands only emerge in the p geometry along both directions, and might constitute the broad feature between 180 and 410 meV below E_F at the Z point along Z-A direction in Figure 3(a). Based on Table 1, these two bands are made of the d_{z^2} and/or d_{xz} orbitals. The ω and ω' bands in other iron-based superconductors were found to be made of d_{z^2} by both experiments and band calculations [13, 23], thus here we could attribute them to the d_{z^2} orbitals as well. However, since the d_{z^2} orbital is mixed with the d_{xz} orbital in the κ band, there should be a finite mixing of the d_{xz} orbital in these two bands.

3 Electronic structure around the zone corner

Previous ARPES studies on $K_xFe_{2-y}Se_2$ superconductors have observed an electron pocket around the zone corner [7, 11, 12], while two electron pockets could be resolved for other iron-based superconductors [16, 17, 23, 24, 28]. In the polarization-dependent photoemission data around the zone

corner (Figure 4), we could observe a shallow electron-like band (δ) with band bottom near −50 meV in both s and p geometries, and a deep electron-like band (δ') in the p geometry which quickly disperses to high binding energies in Figure 4(c) at the temperature of 35 K [33]. Thus the Fermi surface around the zone corner is made of two bands with degenerate Fermi crossings.

The orbital characters of these two bands can be deduced based on the polarization-dependent Fermi surface mappings in Figure 5. In Figures 5(a) and (b), the electron pocket observed in the s geometry has strong intensity at the two vertical positions, while the electron pocket observed in the p geometry has strong intensity at the left horizontal position as summarized in Figure 5(c). The intensity imbalance between the two horizontal positions are due to the matrix element effects caused by the different take-off angles of the photoemission electrons with respect to the incident light. A particular orbital configuration of the Fermi surface would exhibit a characteristic photoemission intensity distribution as simulated in Figure 5(d) for both s and p polarizations. As enforced by the 4-fold symmetry, d_{xz} and d_{yz} would make the two configurations: Conf. #1 and Conf. #2. The observed intense vertical and horizontal sectors under s and p polarizations respectively match the simulated photoemission intensity of Conf. #1. Thus the two horizontal sectors of the

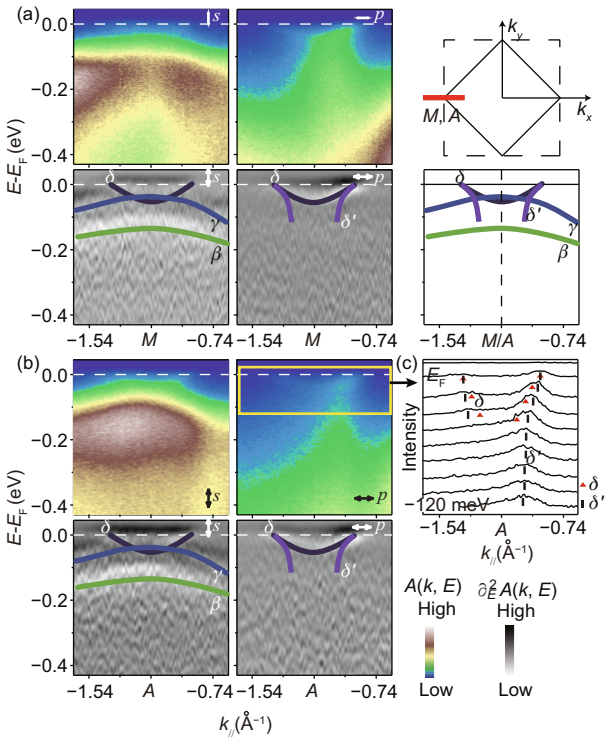

Figure 4 (Color online) The polarization-dependent APRES data around M and A taken with 26 and 36 eV photons, respectively. (a) The photoemission spectra and their corresponding second derivatives with respect to energy taken in the s and p geometries, respectively, along Γ-M direction around M. (b) is the same as the panel (a), but taken along Z-A direction around A. (c) are the MDC's corresponding to the yellow rectangular region in panel (b). The inset is the illustration of the cuts along Γ-M and Z-A directions and the band structure near zone corner.

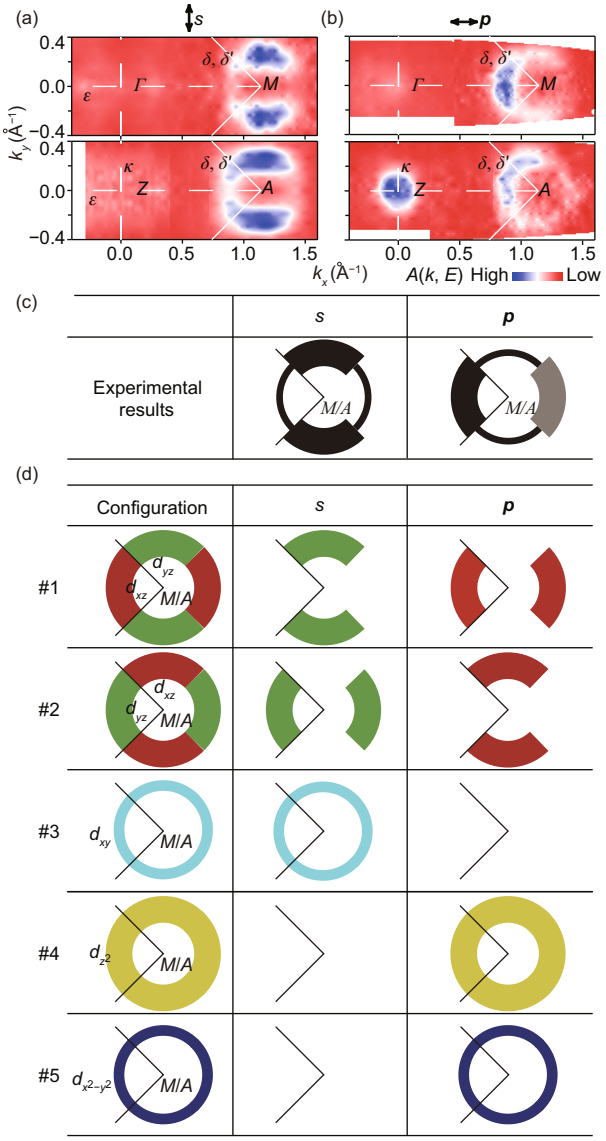

Figure 5 (Color online) The polarization-dependent mapping around Γ, M, Z, and A taken with 21, 26, 30, and 36 eV photons, respectively. (a) and (b) Photoemission intensity maps taken around Γ, M, Z, and A in the s and p geometries, respectively. (c) Summary of the photoemission intensity distributions of the electron pockets around the zone corner. (d) The polarization dependence of the 3d orbitals with different configurations around the zone corner according to the simulated matrix element effects [28]. Based on the four-fold symmetry of the band, the band with d_{xz}, d_{yz}, d_{xy}, $d_{x^2-y^2}$ or d_{z^2} horizontal sectors must have d_{yz}, d_{xz}, d_{xy}, $d_{x^2-y^2}$ or d_{z^2} vertical sectors. The thickness of the line here corresponds to the simulated intensity of each configuration.

electron pockets are mainly contributed by the d_{xz} orbital and the two vertical sectors of the electron pockets are mainly contributed by the d_{yz} orbital, certainly with gradual transitions among them.

However, the complete electron pockets observed in both s and p geometries cannot be explained by just Conf. #1. More orbitals have to be involved. In the p geometry, the two weak vertical sectors should be consisted of even orbitals, such as d_{xz}, $d_{x^2-y^2}$, and d_{z^2}. Based on the band calculations shown in Figure 6, we assume that the electron pockets do not contain any $d_{x^2-y^2}$ and d_{z^2} orbitals, therefore, the two vertical sectors

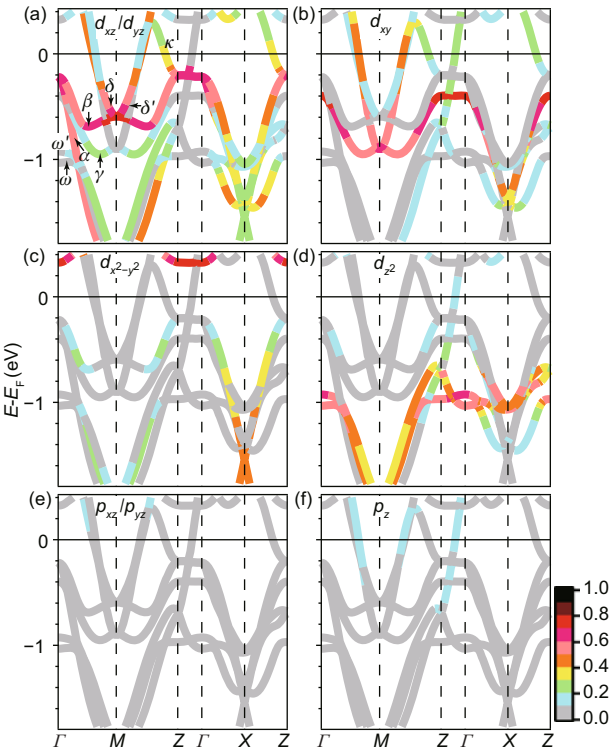

Figure 6 (Color online) Contributions of various Fe 3*d* and Se 4*p* orbitals to the calculated band structure of $K_xFe_{2-y}Se_2$.

has to be of d_{xz}. That is, there is some small contributions from Conf. #2 to the electron cylinders, which explains the weak horizontal sectors in the *s* geometry as well. The intensity distributions of the electron pockets in Figure 5(c) are thus explained by a dominating Conf. #1 plus a small portion of Conf. #2. In Figure 4, since the δ band could be observed in both geometries, it should be made of d_{xz} and d_{yz} in these configurations.

As for the δ' band, its intensity would be rather strong if it had been dominated by the same d_{xz} and d_{yz} orbitals. Considering that the low energy electronic structure at the zone corner is dominated by d_{xy} besides d_{xz} and d_{yz} in the band calculations, δ' would be most likely dominated by the d_{xy} orbital. Since the intensity of simulated matrix element effect of d_{xy} (#3 configuration) is much weaker than that of d_{yz} as shown in Figure 5(d) [28], the overall contributions to the photoemission would still satisfy the observed intensity. On the other hand, the δ' band could be observed in the *p* geometry with weak intensity, and cannot be distinguished in the *s* geometry due to the strong intensity from the β and γ band in Figure 4, it should be dominated by d_{xy} with a small portion of d_{xz}, or Conf. #1. On the other hand, as the d_{xy} orbital is mixed with the d_{xz} orbital in the δ' band, there should be a small portion of the d_{xy} orbital in the δ band as well.

4 Discussion and conclusion

Figure 6 shows the contributions of various Fe 3*d* and Se 4*p* orbitals to the band structure of $K_xFe_{2-y}Se_2$ superconductors by the first-principles calculations, where the full potential linearized augmented plane wave (LAPW) method was implemented in the WIEN2k code [34], using the local density approximation (LDA). The low-energy electronic structure are mostly dominated by the Fe 3*d* orbitals with little contribution from the Se 4*p* orbitals. The bands are labeled in Figure 6(a), following the experimental convention. We note that a band is usually dominated by certain orbital along high symmetry directions, but when away from the high symmetry directions, the band would exhibit some orbital mixing. Moreover, strong orbital mixing would happen when two bands cross with each other or in the transition region between two different orbitals. The strong k_z dispersion of the κ band and two-dimensional character of other bands in Figure 6 agree well with our experiments, thus we only show the summary of the orbital characters along *Z*-*A* direction and the orbital character distributions on the Fermi surface around Γ, *M*, *Z*, and *A* (Figure 7). Although the band calculations well capture most of our experimental results, there are still a few discrepancies. For example, the band calculations miss the orbital character of the κ band that contributes to the Fermi surface. Experimentally, the κ band is found to be mainly made of d_{z^2} with just a trace of d_{xz}/d_{yz}, while it is dominated by d_{xz}/d_{yz} in the calculations. A previous ARPES study suggests that the κ band is the mixture of the Se 4*p* and Fe 3*d* orbitals [35]. Although our calculations show a minimal involvement of the Se 4*p* orbitals, our polarization-dependent study cannot distinguish the Se $4p_z$ from the Fe $3d_{z^2}$ orbitals, thus we leave this issue open.

Interestingly, the η and ϵ bands observed in the experiment are not found in the calculations. It is likely that the η band might be a surface state. As shown in Figures 7 and 8, the δ and ε bands have similar Fermi surface pocket and dispersion behavior, except the intensity of the ϵ band is much weaker. It seems that the ε band is folded from the δ band, which should

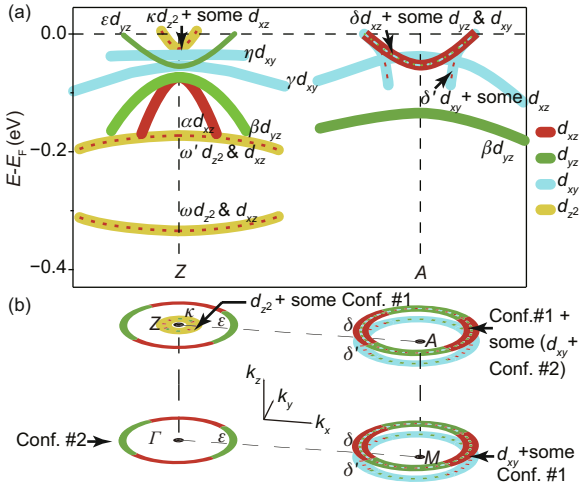

Figure 7 (Color online) (a) The summary of the orbital characters of low-energy electronic structure in $K_xFe_{2-y}Se_2$ superconductor along *Z*-*A* direction. (b) The illustration of the orbital characters on the Fermi surface sheets around Γ, *M*, *Z*, and *A*. The overlapping δ and δ' Fermi surface sheets around *M* and *A* are separated for a better illustration.

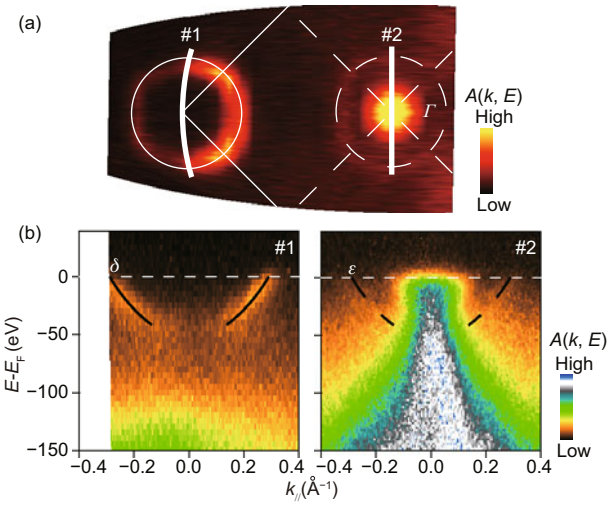

Figure 8 (Color online) APRES data around Γ taken with 21 eV photon at SSRL. (a) Photoemission intensity map taken around Γ. (b) The photoemission spectra along cuts #1 and #2, respectively.

be originated from the $\sqrt{2} \times \sqrt{2}$ ordering in $K_xFe_{2-y}Se_2$ superconductor revealed in the scanning tunneling microscopy (STM) and transmission electron microscopy (TEM) studies [36, 37]. However, the ϵ band could only be observed in the s geometry, while the δ bands could be observed in both geometries. Such an orbital-dependent folding may require further theoretical and experimental studies.

To summarize, we have carried out a systematic investigation of orbital characters in $K_xFe_{2-y}Se_2$ superconductor based on the strong polarization-dependent photoemission response of the low-energy electronic structure. The α, β, γ, δ, and δ' bands are dominated by similar orbitals in $K_xFe_{2-y}Se_2$ and other iron-based superconductors [27, 28]. However, the δ and δ' bands are weakly hybridized in $K_xFe_{2-y}Se_2$, instead of being strongly hybridized in the other iron-based superconductors. Besides, the κ and ϵ Fermi surfaces have only been reported in $K_xFe_{2-y}Se_2$ superconductor. Moreover, the κ band exhibits the d_{z^2} orbital character, which is different from the band calculations, while the ϵ band, which is not predicted in the band calculations, is made of the d_{yz} orbital. These explicit conclusions on the orbital characters of the band structure would help understand the unique properties of $K_xFe_{2-y}Se_2$.

The authors thank D. H. Lu for the experimental assistance at SSRL. This work was supported in part by the National Natural Science Foundation of China, Ministry of Education of China, and the National Basic Research Program of China (2012CB921400, 2011CB921802 and 2011CBA00112). SSRL is operated by the US Department of Energy, Office of Basic Energy Science, Divisions of Chemical Sciences and Material Sciences.

1 Guo J G, Jin S F, Wang S C, et al. Superconductivity in the iron selenide $K_xFe_{2-y}Se_2$ ($0 \leqslant x \leqslant 1.0$). Phys Rev B, 2010, 82: 180520
2 Luo Y K, Li Y K, Jiang S, et al. Phase diagram of $CeFeAs_{1-x}P_xO$ obtained from electrical resistivity, magnetization, and specific heat measurements. Phys Rev B, 2010, 81: 134422
3 Hu W Z, Li G, Zheng P, et al. Optical study of the spin-density-wave properties of single-crystalline $Na_{1-\delta}FeAs$. Phys Rev B, 2009, 80: 100507
4 Hu W Z, Dong J, Li G, et al. Origin of the spin density wave instability in AFe_2As_2 (A=Ba,Sr) as revealed by optical spectroscopy. Phys Rev Lett, 2008, 101: 257005
5 Yan Y J, Zhang M, Wang A F, et al. Electronic and magnetic phase diagram in $K_xFe_{2-y}Se_2$ superconductors. Sci Rep, 2012, 2: 212
6 Craco L, Laad M S, Leoni S, et al. Unconventional Mott transition in $K_xFe_{2-y}Se_2$. arXiv: 1109.0116v1
7 Chen F, Xu M, Ge Q Q, et al. Electronic identification of the parental phases and mesoscopic phase separation of $K_xFe_{2-y}Se_2$ superconductors. Phys Rev X, 2011, 1: 021020
8 Chen Z G, Yuan R H, Dong T, et al. Infrared spectrum and its implications for the electronic structure of the semiconducting iron selenide $K_{0.83}Fe_{1.53}Se_2$. Phys Rev B, 2011, 83: 220507
9 Cao C, Dai J H. Electronic structure of KFe_2Se_2 from first-principles calculations. Chin Phys Lett, 2011, 28: 057402
10 Li W, Ding H, Deng P, et al. Phase separation and magnetic order in K-doped iron selenide superconductor. Nat Phys, 2012, 8: 126–130
11 Zhang Y, Yang L X, Xu M, et al. Nodeless superconducting gap in $K_xFe_2Se_2$ (A=K,Cs) revealed by angle-resolved photoemission spectroscopy. Nat Mater, 2011, 10: 273–277
12 Mou D X, Liu S Y, Jia X W, et al. Distinct Fermi surface topology and nodeless superconducting gap in a $(Tl_{0.58}Rb_{0.42})Fe_{1.72}Se_2$ superconductor. Phys Rev Lett, 2011, 106: 107001
13 Yang L X, Xie B P, Zhang Y, et al. Surface and bulk electronic structures of LaFeAsO studied by angle-resolved photoemission spectroscopy. Phys Rev B, 2011, 82: 104519
14 Yang L X, Zhang Y, Ou H W, et al. Electronic structure and unusual exchange splitting in the spin-density-wave state of the $BaFe_2As_2$ parent compound of iron-based superconductors. Phys Rev Lett, 2009, 102: 107002
15 Zhang Y, Wei J, Ou H W, et al. Unusual doping dependence of the electronic structure and coexistence of spin-density-wave and superconductor phases in single crystalline $Sr_{1-x}K_xFe_2As_2$. Phys Rev Lett, 2009, 102: 127003
16 He C, Zhang Y, Xie B P, et al. Electronic-structure-driven magnetic and structure transitions in superconducting NaFeAs single crystals measured by angle-resolved photoemission spectroscopy. Phys Rev Lett, 2010, 105: 117002
17 Chen F, Zhou B, Zhang Y, et al. Electronic structure of $Fe_{1.04}Te_{0.66}Se_{0.34}$. Phys Rev B, 2010, 81: 014526
18 Kuroki K, Onari S, Arita R, et al. Unconventional pairing originating from the disconnected Fermi surfaces of superconducting $LaFeAsO_{1-x}F_x$. Phys Rev Lett, 2008, 101: 087004
19 Graser S, Maier T A, Hirschfeld P J, et al. Near-degeneracy of several pairing channels in multiorbital models for the Fe pnictides. New J Phys, 2009, 11: 025016
20 Ran Y, Wang F, Zhai H, et al. Nodal spin density wave and band topology of the FeAs-based materials. Phys Rev B, 2009, 79: 014505
21 Zhang Y, Ye Z R, Ge Q Q, et al. Nodal superconducting-gap structure in ferropnictide superconductor $BaFe_2(As_{0.7}P_{0.3})_2$. Nat Phys, 2012, 8: 371–375
22 Damascelli A, Hussain Z, Shen Z X. Angle-resolved photoemission studies of the cuprate superconductors. Rev Mod Phys, 2003, 75: 473–541
23 Zhang Y, Chen F, He C, et al. Orbital characters of bands in the iron-based superconductor $BaFe_{1.85}Co_{0.15}As_2$. Phys Rev B, 2011, 83: 054510
24 Ye Z R, Zhang Y, Xu M, et al. Phosphor induced significant hole-doping

in ferropnictide superconductor $BaFe_2(As_{1-x}P_x)_2$. arXiv: 1105.5242v1

25 Zhang Y, Yang L X, Chen F, et al. Out-of-plane momentum and symmetry-dependent energy gap of the pnictide $Ba_{0.6}K_{0.4}Fe_2As_2$ superconductor revealed by angle-resolved photoemission spectroscopy. Phys Rev Lett, 2010, 105: 117003

26 Wray L A, Hsieh D, Xia Y, et al. Observation of intertwined Fermi surface topology, orbital parity symmetries and electronic interactions in iron arsenide superconductors. arXiv: 0912.5089v1

27 Wang X P, Richard P, Huang Y B, et al. Orbital characters determined from Fermi surface intensity patterns using angle-resolved photoemission spectroscopy. arXiv: 1201.3655v1

28 Zhang Y, He C, Ye Z R, et al. Symmetry breaking via orbital-dependent reconstruction of electronic structure in detwinned NaFeAs. Phys Rev B, 2012, 85: 085121

29 Yi M, Lu D H, Moore R G, et al. Electronic reconstruction through the structural and magnetic transitions in detwinned NaFeAs. arXiv: 1111.6134v1

30 Khodas M, Chubukov A V. Inter-pocket pairing and gap symmetry in Fe-based superconductors with only electron pockets. arXiv: 1202.5563v1

31 Xu M, Ge Q Q, Peng R, et al. Evidence for an s-wave superconducting gap in $K_xFe_{2-y}Se_2$ from angle-resolved photoemission. Phys Rev B, 2012, 85: 220504

32 Wang A F, Ying J J, Yan Y J, et al. Superconductivity at 32 K in single-crystalline $Rb_xFe_{2-y}Se_2$. Phys Rev B, 2011, 83: 060512

33 Shen Z X. Private communication

34 Blaha P, Schwarz K, Madsen G K H, et al. WIEN2k: An augmented plane wave plus local orbitals program for calculating crystal properties. User's Guide. Vienna: Vienna University of Technology, 2001

35 Liu Z H, Richard P, Xu N, et al. Three-dimensionality and orbital characters of Fermi surface in $(Tl,Rb)_yFe_{2-x}Se_2$. arXiv: 1202.6417v2

36 Cai P, Ye C, Ruan W, et al. Imaging the coexistence of a superconducting phase and a charge-density modulation in the $K_{0.73}Fe_{1.67}Se_2$ superconductor using a scanning tunneling microscope. Phys Rev B, 2012, 85: 094512

37 Li J Q, Song Y J, Yang H X, et al. Collapse of the Fe-vacancy order and successive phase transitions in superconducting $K_xFe_{2-y}Se_2$ ($0.7\leqslant x\leqslant 0.8$, $0.2\leqslant y\leqslant 0.3$). arXiv: 1104.5340v1